Science Advances
AAAS

advances.sciencemag.org/cgi/content/full/5/9/eaaw6490/DC1

Supplementary Materials for

Structural basis of sterol recognition by human hedgehog receptor PTCH1

Chao Qi, Giulio Di Minin, Irene Vercellino, Anton Wutz, Volodymyr M. Korkhov*

*Corresponding author. Email: volodymyr.korkhov@psi.ch

Published 18 September 2019, *Sci. Adv.* **5**, eaaw6490 (2019)
DOI: 10.1126/sciadv.aaw6490

The PDF file includes:

Other Supplementary Material for this manuscript includes the following:

(available at advances.sciencemag.org/cgi/content/full/5/9/eaaw6490/DC1)

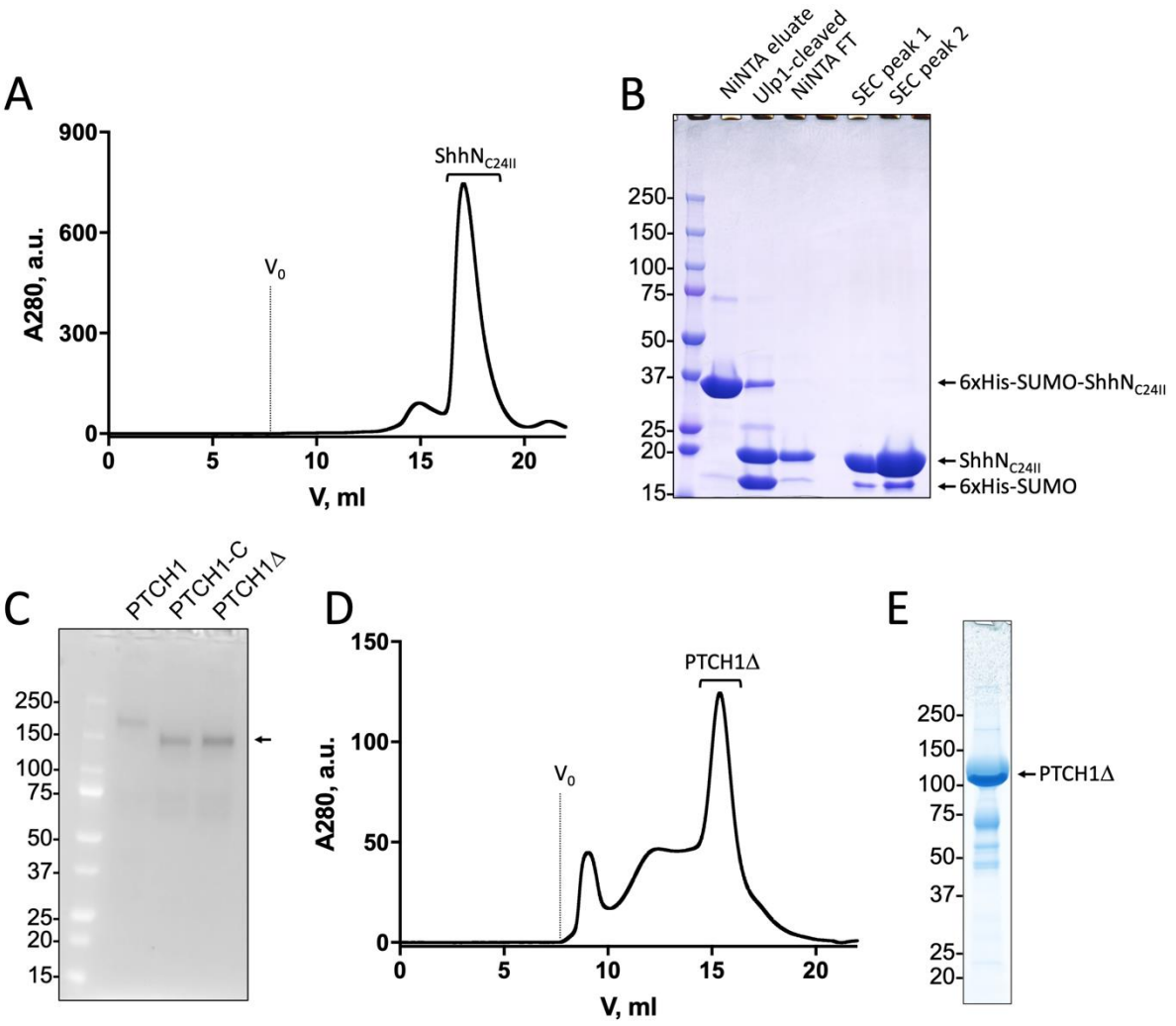

Fig. S1. Purification of the hedgehog ligand and PTCH1. A. Size exclusion chromatography (SEC) profile of the $ShhN_{C24II}$ protein; SEC was performed using Superdex 200 10/300 GL Increase column. The void volume is indicated by "V_0"; fractions chosen for complex reconstitution are indicated by a bracket. B. SDS PAGE analysis of the key stages of $ShhN_{C24II}$ purification. The fractions loaded on the gel were applied as indicated in the gel; Ulp1 is the SUMO protease; "NiNTA FT" is NiNTA flow-through after Ulp1 cleavage; "SEC Peak 1/2" indicate 3 μl and 10 μl of the same SEC peak (A), respectively. C. In gel fluorescence analysis of the SDS PAGE gel resolving the following samples: "PTCH1" – GFP-labeled full-length wild-type PTCH1; "PTCH1-C" – GFP-labeled C-terminal truncation of PTCH1 (residues 1-1188); "PTCH1Δ" the final construct used for structure determination (residues 1-1188, containing a Y645A mutation). Position of the truncated protein is indicated by an arrow. D. SEC profile of the purified PTCH1Δ preparation. SEC was performed using Superose 6 10/300 GL Increase column. E. SDS PAGE of the final PTCH1 sample.

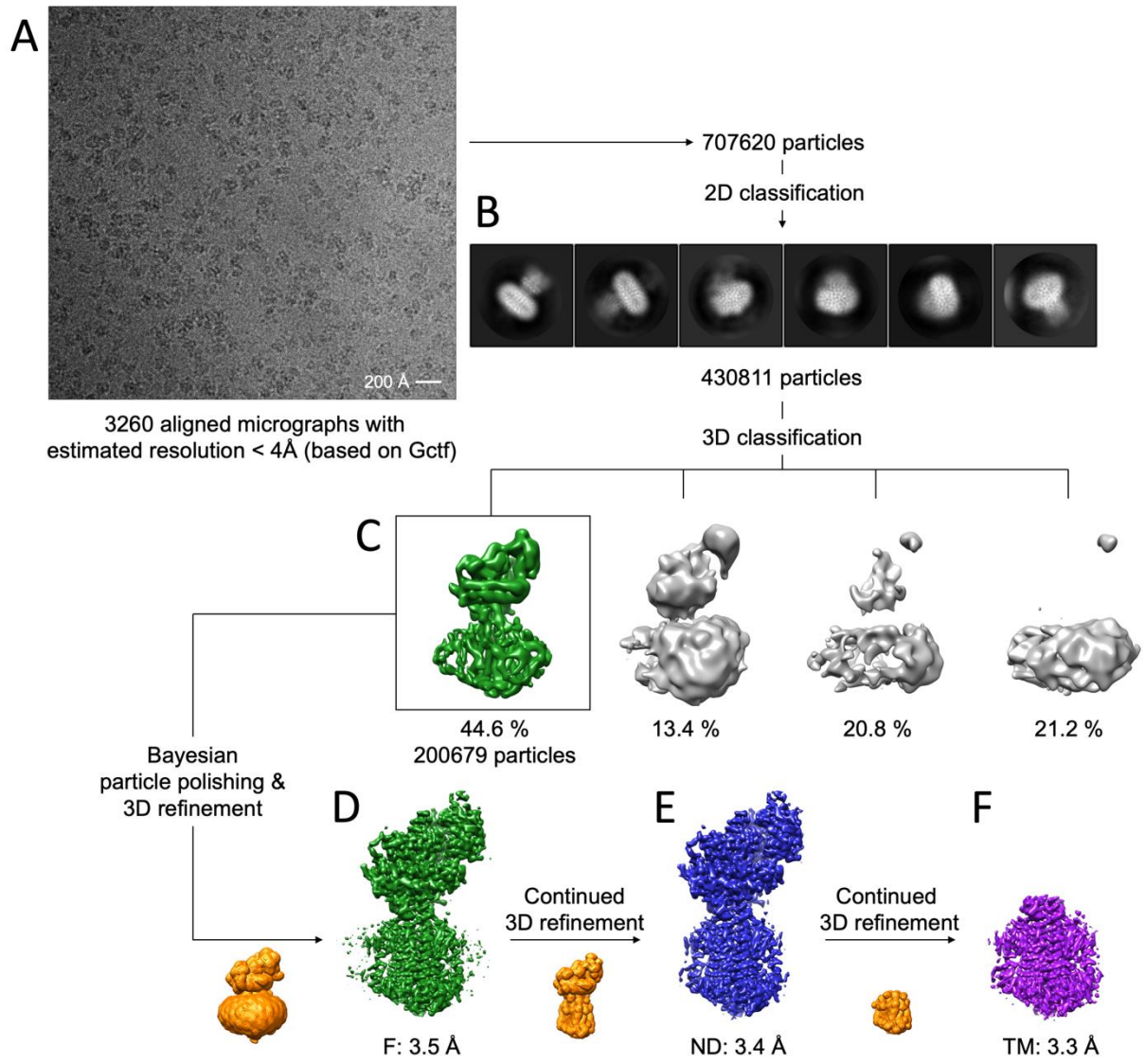

Fig. S2. Cryo-EM and single-particle analysis workflow. A. The aligned averaged micrograph shows a high quality monodisperse sample of the PTCH1Δ-ShhN$_{C24II}$ complex in digitonin. B. The best 2D classes calculated in relion-2.0.b prior to the 3D classification step; 2D class features appear blurred. C. The 3D classification job with 4 classes resulted in a single class with clearly defined secondary structure elements. This class was subjected to further processing using relion-2.0.b and relion-3.0. D. Refinement of the best 3D class after Bayesian particle polishing in relion-3.0 (detailed in the "Material and Methods"), using a mask encompassing the complete complex (orange) resulted in a postprocessed density map at 3.5 Å resolution (full map, green, "F"; FSC 0.143). E. Continued refinement of the same dataset, substituting the full mask with a modified mask excluding the detergent micelle density resulted in a postprocessed map 3.4 Å resolution (no-detergent map, blue, "ND"). F. Continued refinement following the ND map, using the mask covering only the transmembrane region of PTCH1Δ resulted in the postprocessed map at 3.3 Å resolution (transmembrane map, magenta, "TM"). For each map, sharpening with a b-factor of -50 was used in the postprocessing step.

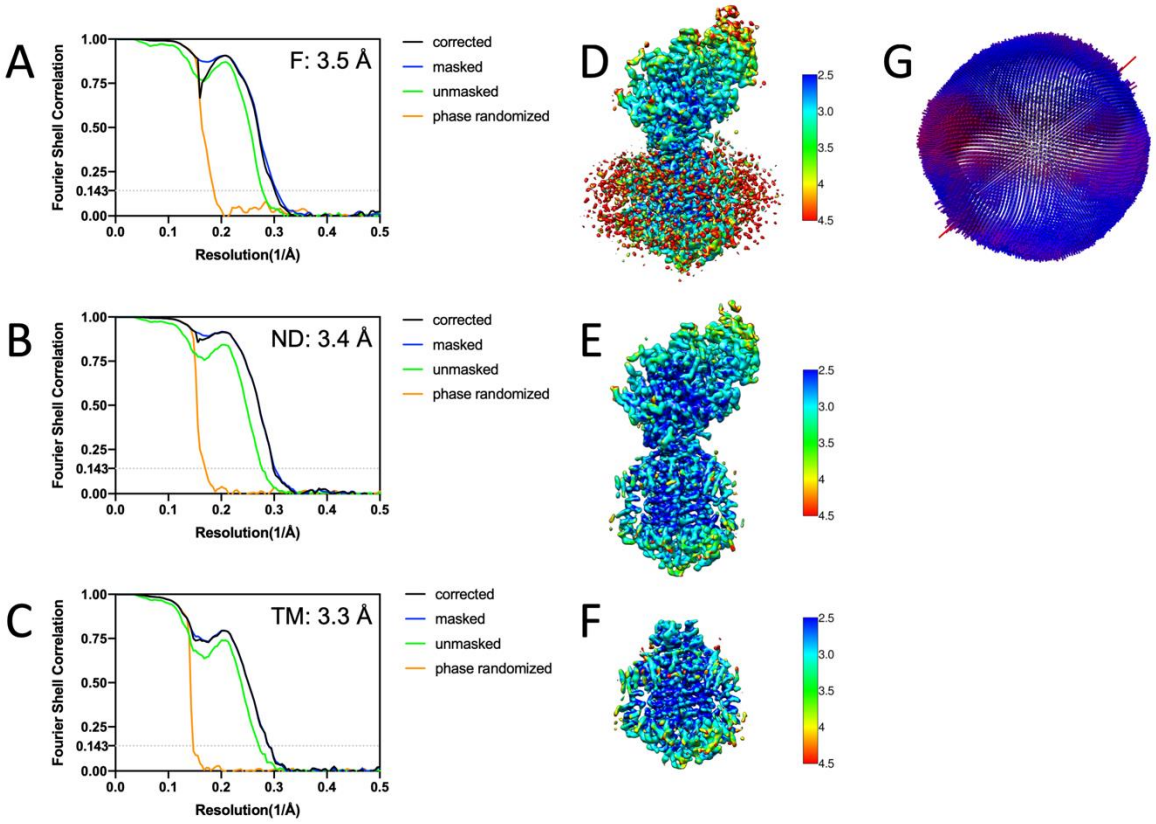

Fig. S3. FSC plots and 3D reconstruction details. A-C. FSC plots for the three maps, "F", "ND" and "TM" (as defined in fig. S2), calculated in relion-3.0. The dotted line indicates the 0.143 threshold ("gold standard FSC"). D-F. Local resolution estimates, calculated using ResMap implemented in relion-3.0. The scale bars indicate the resolution, scaled between 2.5 Å (blue) and 4.5 Å (red). G. Angular distribution of the refined dataset (calculated in relion-3.0 using the data in A and D).

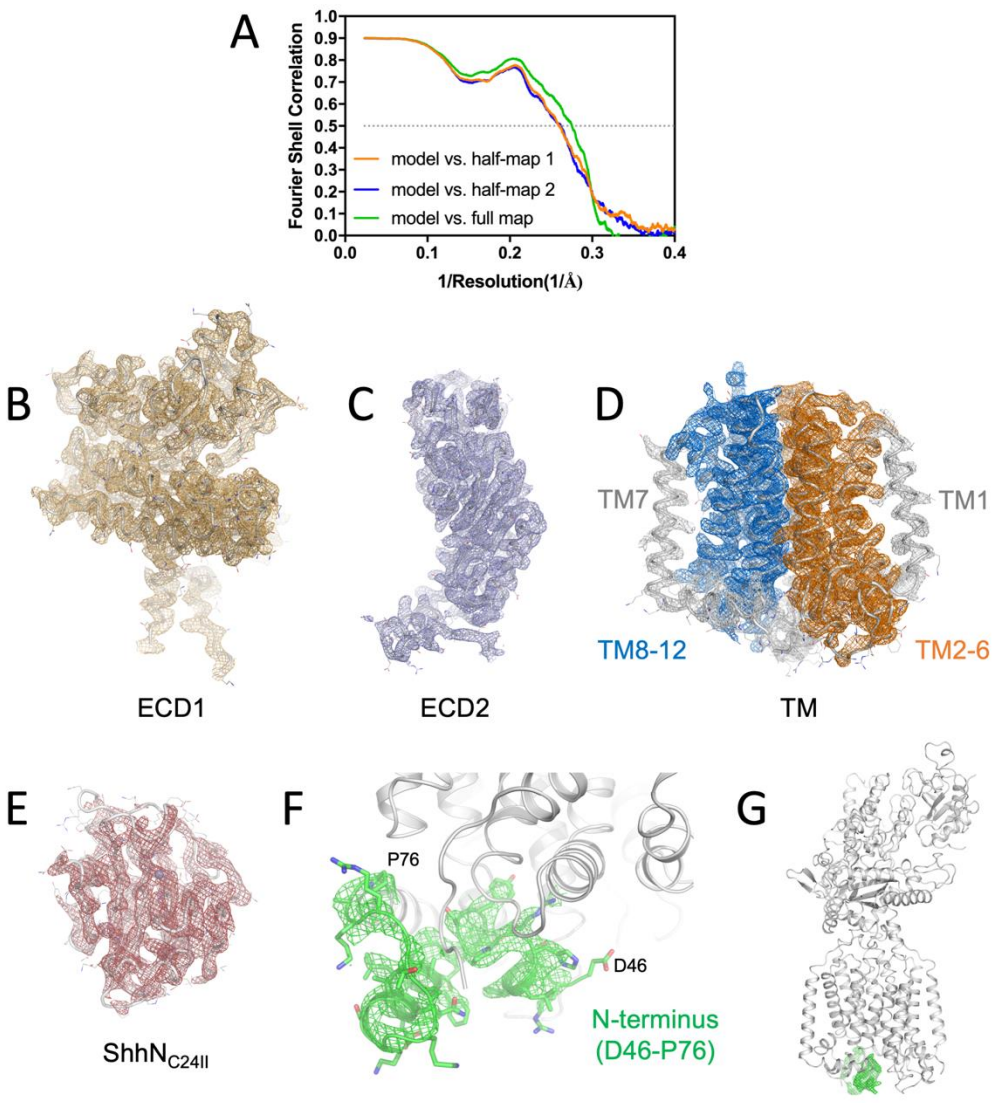

Fig. S4. Features of the map and the atomic model of the protein. A. Model to map FSC, calculated as detailed in "Materials and Methods"; the full statistics for the model are shown in Table S1. B-E. Individual parts of the map shown as mesh, including the regions corresponding to ectodomain 1 ("ECD1"), ectodomain 2 ("ECD2"), complete transmembrane domain bundle ("TM") and the modified hedgehog ligand ShhN$_{C24II}$. The protein model is shown as ribbon, with side-chain represented with lines (colored by atom type). F. The N-terminal residues of PTCH1Δ (D46-P76) resolved in our 3D reconstruction are shown as green mesh. G. The N-terminus forms an interface with the cytosolic side of the SSD and SSDL portions of the protein.

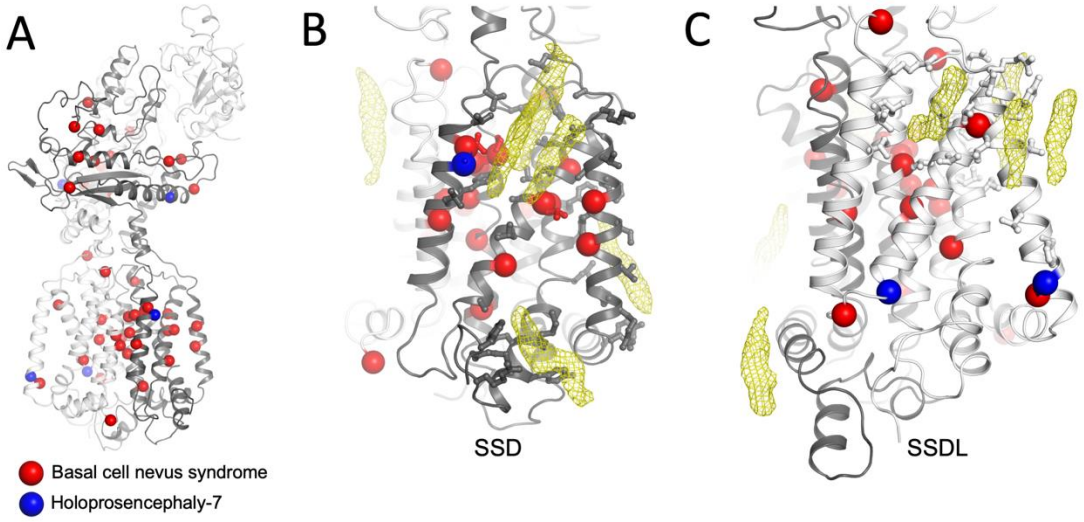

Fig. S5. Disease-linked mutations in PTCH1 are present within the SSD and SSDL regions of the protein. A. Overview of the structure with the mutation sites linked to basal cell nevus syndrome (BCNS; red) and holoprosencephaly-7 (HPE-7; blue) indicated with spheres (Cα atoms only). B-C. The views of the SSD (B) and SSDL (C) region show the positions of the disease-linked residues (spheres), with sterol binding site residue side-chains shown as sticks. Side chains that match residues linked to disease are coloured accordingly. Positions corresponding to the bound sterols in the TM density map are shown as yellow mesh.

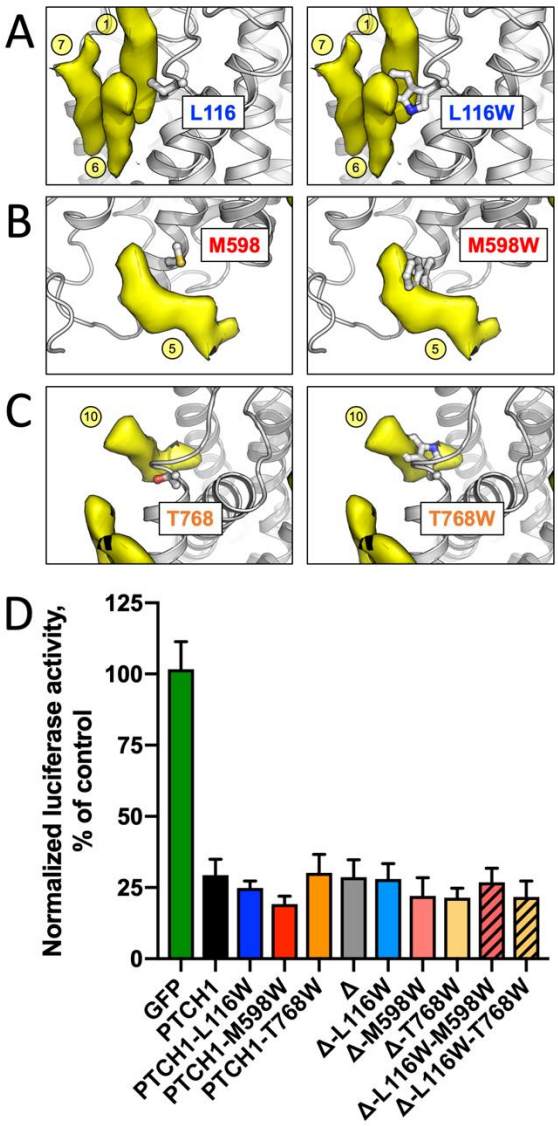

Fig. S6. Mutations designed to disrupt sterol binding sites in PTCH1 fail to suppress hedgehog pathway activation. A-C. The views of the residues L116 (A), M598 (B) and T768 (C), chosen for substitution to a bulky residue (W); the models of the mutants, illustrating the disruption of the sterol sites (represented using the yellow density map and labelled with the numbered circles), were generated using PyMol. D. The luciferase-based reporter assay for hedgehog pathway activation shows that all PTCH1 and PTCH1Δ (indicated by "Δ") constructs are capable of inhibiting the pathway in transiently transfected PTCH1-/- mouse embryo fibroblasts. All values, including the GFP control, were normalized using the measurements performed using the cells transfect with the empty expression vector. For all measurements, n = 4; for measurements with full-length PTCH1 and mutants, n = 3. All values are significantly different from the GFP control, but not different from each other, based on one way ANOVA ($P < 0.001$).

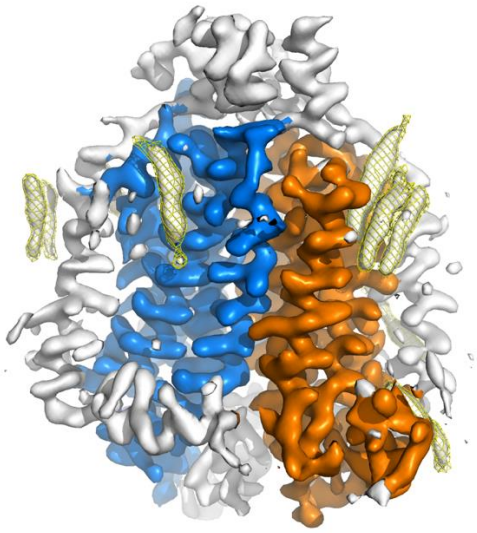

Movie S1. The density elements corresponding to bound sterols in the PTCH1 TM-focused map. The movie was generated in Pymol (mset and util.mroll commands with 180 frames), using the TM map shown in Fig. 2B. The map is coloured according to Fig. 2B (SSD is coloured orange, SSDL is coloured blue). The positions of the sterol sites are indicated by yellow mesh over the density map.

Table S1. Cryo-EM data collection, single-particle analysis, and model building statistics.

Data collection	
Instrument	FEI Titan Krios / Gatan K2 Summit / Quantum GIF
Magnification	61425 (165kx)
Voltage (kV)	300
Electron exposure ($e^-/Å^2$)	44.7
Defocus range (um)	-0.8 to -2.4
Pixel size (Å)	0.814
Resolution (Å; FSC 0.143)	3.5 (F), 3.4 (ND), 3.3 (TM)
Number of particles	200679
Model refinement	
Model resolution (FSC 0.5; ND)	3.63
Map sharpening b-factor (Å)	-50
Map CC	0.775
Model composition	
protein residues/ligands	1195/19
B factor ($Å^2$)	101.45
Bond length RMSD (Å)	0.01
Bond angle RMSD (°)	0.91
Validation	
MolProbity score	1.71
Clash score	4.15
Rotamer outliers (%)	0.10
Ramachandran plot	
Favored (%)	91.28
Allowed (%)	8.72
Disallowed (%)	0.0